JOURNAL OF GUIDANCE, CONTROL, AND DYNAMICS
Vol. 27, No. 4, July–August 2004

Computation of Controllability Regions for Unstable Aircraft Dynamics

M. G. Goman* and M. N. Demenkov†
De Montfort University, Leicester, England LE1 9BH, United Kingdom

An active control approach to air vehicle design can significantly expand the flight envelope and improve vehicle performance characteristics. In some cases it can be attained by implementing the aerodynamically unstable configuration or expanding operation at flight regimes with dynamic instability, which are then purposely stabilized by the flight control system. An important issue in stabilization of unstable dynamics is connected with the size of the controllability region, which is the set of all states of the aircraft dynamics that can be stabilized by some realizable control action. This region is bounded because of nonlinear actuator constraints, and its size can be considered as a measure for allowable level of external disturbances. In this paper an algorithm based on convex optimization technique is proposed for computation of the controllability region of an unstable linear system under amplitude and rate control constraints. Examples of the controllability region analysis for an aeroservoelastic airfoil system and unstable aircraft dynamics are presented to illustrate the capabilities of the proposed algorithm.

Nomenclature

$C, \partial C$	=	controllability region and its boundary
$C(N)$	=	null-controllable region at step N for discrete-time system
$C(T)$	=	null-controllable region at time T for continuous-time system
$\bar{c}$	=	mean aerodynamic chord
c_h, c_m, c_δ	=	nondimensional aerodynamic coefficients for the normal force and pitch and flap hinge moments
c_w	=	unsteady aerodynamic contribution to the normal-force coefficient
h	=	plunge displacement
$\bar{h}, \dot{\bar{h}}$	=	nondimensional plunge displacement and its reduced time derivative
I	=	identity matrix
I_θ, I_δ	=	generalized masses of the pitch and flap dynamic modes
k_h, k_θ, k_δ	=	structural stiffness coefficients in plunge, pitch, and flap deflections
m_a	=	generalized mass of the plunge dynamic mode
P, Q, R	=	roll, pitch, and yaw rates
R^n	=	n-dimensional Euclidean space
$R^{n\times m}$	=	$n \times m$ real matrix
S	=	wing area
$s_{h\theta}, s_{h\delta}, s_{\theta\delta}$	=	inertial coupling between the generalized coordinates
U	=	flow speed
V	=	aircraft velocity
$[x; y]$	=	$[x^T \;\; y^T]^T$
(x_i, x_j)	=	two-dimensional plane spanned by axes x_i and x_j
$0_{m\times n}$	=	$m \times n$ matrix of zeros
α, β	=	angle of attack and sideslip angle
$\delta, \dot{\delta}$	=	trailing-edge flap deflection and its reduced time derivative
$\delta_c, \dot{\delta}_c$	=	control command and its reduced time derivative
$\delta_{\text{rbf}}, \delta_{\text{lbf}}$	=	right and left body flaps deflections
$\delta_{\text{revi}}, \delta_{\text{levi}}$	=	right and left inboard elevons deflections
$\delta_{\text{revo}}, \delta_{\text{levo}}$	=	right and left outboard elevons deflections
$\delta_{\text{rvr}}, \delta_{\text{lvr}}$	=	right and left rudders deflections
$\theta, \dot{\theta}$	=	pitch angle and its reduced time derivative
ρ	=	air density
ϕ, ψ	=	bank and heading angles
$\omega_h, \omega_\theta, \omega_\delta$	=	reduced plunge, pitch, and flap natural frequencies
$\omega_{\theta_{\text{fl}}}$	=	reduced pitch frequency at flutter boundary

Introduction

AN aerodynamically unstable aircraft configuration stabilized by a control system has a potential to overcome many conventional design limitations. For example, such an aircraft configuration can possess a higher lift-to-drag ratio, the critical flight regimes associated with high incidence departures or aeroelastic instabilities can be significantly relaxed or even eliminated by implementation of control system. Hence, the active control approach to air vehicle design grants the opportunity for improvement of air vehicle dynamic and performance characteristics.

At flight regimes with dynamic instability, aircraft motion can be locally represented by linear time invariant system with unstable eigenvalues. In this case the important problem in design of control laws is connected with realistic account of actuator constraints such as deflection limits and rate saturation.[1,2]

The unstable linear system with constrained control inputs has a bounded controllability region,[3–5] which means that the stabilization problem under the restriction on control input can be solved only for a limited set of initial states of the system.

The size of the controllability region for the open-loop unstable system with constrained control inputs can serve as a controllability measure for the control design problem. If external disturbances move the system out the controllability region, no controller is able to keep the system stable.

The stability region (or domain of attraction) for the closed-loop system by definition is the set of states that are stabilizable by a particular controller. The stability region generally utilizes only a part of the open-loop system controllability region and never can exceed it. In some cases a "good" controller in terms of linear system criteria such as local stability and robust performance can provide the closed-loop system with very small and unsatisfactory stability region. Therefore, the additional design objective can be formulated

Presented as Paper 2002-4749 at the AIAA Guidance, Navigation, and Control Conference, Monterey, CA, 5–8 August 2002; received 28 July 2003; revision received 3 November 2003; accepted for publication 5 November 2003.

*Professor, Faculty of Computing Sciences and Engineering, Hawthorn Building, The Gateway; mgoman@dmu.ac.uk. Member AIAA.

†Ph.D. Candidate, Faculty of Computing Sciences and Engineering, Hawthorn Building, The Gateway; mdemenkov@mail.ru. Student Member AIAA.

as maximizing the region of attraction for the closed-loop system. This objective maximizes the level of external disturbances, which can be rejected by the system.

It is necessary to bear in mind that various design methods lead to different stability regions for the closed-loop system. A ratio between stability region and controllability region can be considered as an additional performance measure for assessment of controller robustness to external disturbances.

The main objective of this work was in developing of the computational algorithm for analysis of the controllability region for unstable aircraft dynamics in the presence of actuator constraints such as amplitude and rate saturation. The first part contains a description of the proposed computational algorithm, which is based on the solution of a linear programming problem. In the second part this algorithm is applied to an active control flutter suppression problem and to a stabilization problem of unstable lateral/directional aircraft dynamics.

Background and Problem Statement

Let us consider the following open-loop unstable continuous-time system:

$$\dot{x}(t) = Ax(t) + Bu(t) \tag{1}$$

where $A \in R^{n\times n}$ has eigenvalues with positive real parts, $B \in R^{n\times m}$, $x \in R^n$, and $u \in R^m$. It is additionally supposed that the state vector x is fully observable and $n > 1$.

We will study the effect on system dynamics of both amplitude and rate control constraints:

$$u_{\min} \le u \le u_{\max} \tag{2a}$$

$$\dot{u}_{\min} \le \dot{u} \le \dot{u}_{\max} \tag{2b}$$

Here the inequalities are treated component-wise.

Although the stability of an equilibrium in a linear system is a global property, the stability of an equilibrium in a nonlinear system is just a local characteristic. The unstable linear system in Eq. (1) under any control law with inputs constrained as in Eq. (2a) becomes nonlinear and can be stable only in a bounded region of the state space, known as stability region or region of attraction. The maximum attainable region of attraction coincides with the controllability region, which is also called the asymptotically null controllable region.[3–5]

Rate constraints given in Eq. (2b) preserve continuity of the control function. In this case the reachability of the origin from some initial states of the system depends on the initial positions of actuators. This means that the controllability region of the open-loop system and the stability region for the closed-loop system must be defined in the extended state + control space.

Note that a control function $u(t)$ which satisfies only deflection constraints (2a) can be discontinuous. The controllability and stability regions in this case can be specified only in the system state space because the reachability of the origin from any initial state does not depend on initial values of control vector. In some cases a control function $u(t)$ steering an initial state from the controllability region to the origin can be of the bang-bang type,[3,5] that is, piecewise constant and discontinuous. The possibility of discontinuous control significantly simplifies the computation of the controllability region.

The more rigorous description of the controllability region given next is needed for derivation of the computational algorithm, which is presented in the following section.

By definition, an extended state $[x_0; u_0]$ is asymptotically null controllable if there exists a control function $u(t)$ that satisfies constraints in Eq. (2) and generates the state trajectory with initial conditions $x(0) = x_0$ and $u(0) = u_0$, so that the state and control asymptotically approach the origin as $t \to \infty$:

$$\lim_{t\to\infty} x(t) = 0, \qquad \lim_{t\to\infty} u(t) = 0 \tag{3}$$

The set of all extended states $[x_0; u_0] \in R^{n+m}$ that are asymptotically null controllable is called the controllability region for the system and denoted by $C \in R^{n+m}$. It can be easily shown that this region is convex.

Controllability Region Analysis: Known Approaches

The controllability region of a linear system defined in Eq. (1) with only amplitude control constraints has been studied by Formal'skii,[3] Goman et al.,[4] Goman and Demenkov,[6] and Hu and Lin.[5] (In the latter work the controllability region is called the asymptotically null controllable region.) Several geometrical properties of the controllability region have been revealed in these works, and some methods for explicit characterization of the controllability region have been proposed.

All eigenvalues $\lambda_i, i = 1, \ldots, n$ of matrix A in Eq. (1) can be divided into stable ($Re\lambda_i < 0$), neutral ($Re\lambda_i = 0$), and antistable ($Re\lambda_i > 0$) groups. Here $Re\lambda_i$ is the real part of λ_i.

If matrix A has only antistable eigenvalues, then the controllability region $C \in R^n$ of the system in Eq. (1) is strictly convex and overall bounded.[3,5] As a result, if the unstable system has some antistable eigenvalues it cannot be stabilized in the full state-space R^n because it contains antistable subsystem with bounded controllability region.

Computation of controllability region C can be performed by reconstruction of its boundary ∂C formed by invariant manifold of system trajectories under the bang-bang control.[4,5] It has been shown that trajectories on ∂C satisfy Pontryagin's minimum principle[7] and can contain unstable equilibrium points and closed orbits.[4,5]

The boundaries of stability and controllability regions for a two-dimensional system with only antistable eigenvalues and scalar limited control input $|u(t)| \le u_{\max}$ have been analyzed in Ref. 4 considering the bang-bang control. The geometric properties of the boundary trajectories have been investigated using bifurcation analysis methods. Later similar results have been independently obtained in Ref. 5 with the rigorous proof of the boundary trajectories properties.

An optimization-based method for explicit description of the controllability region boundary can be found in Refs. 3 and 5. It was applied for antistable (i.e., having only antistable open-loop eigenvalues) linear systems under only amplitude constraints (2a).

The main idea of this method is based on maximization of a scalar linear function $f(x) = \eta^T x$ ($\eta \in R^n$, $\eta \ne 0$) over all points x from the controllability region. The maximization process is performed along the specified direction η, so that the final solution coincides with the point $x_b(\eta)$ on the boundary of the controllability region. Because the controllability region for antistable system with only amplitude constraints is strictly convex and overall bounded, this solution always exists, and it is unique. The vector η defines supporting hyperplane at this boundary point x_b.

For numerical computation of the controllability region boundary, the null-controllable region at time T, denoted as $C(T)$, is introduced. It is defined as the set of states that can be steered to the origin in a finite time T by application of amplitude constrained control $u(t)$.

The boundary points of $C(T)$ in this case can be explicitly expressed as follows:

$$x_b(\eta) = \arg\max_{x\in C(T)} \eta^T x$$

$$= -\sum_{i=1}^{m} \int_0^T e^{-A\tau} b_i u_{i\,\max} \operatorname{sign}\left(-\eta^T e^{-A\tau} b_i\right) d\tau \tag{4}$$

where b_i is the ith column of matrix B (also we suppose for simplicity that $u_{i\,\max} = -u_{i\,\min}$).

The optimization problem in Eq. (4) can be solved for different directions η, and the obtained points $x_b(\eta)$ can approximate rather accurately the controllability region boundary ∂C as $T \to \infty$.

Problem Statement

Different controllers in the closed-loop system produce stability regions having different size, which never exceeds the size of the

controllability region. So, the ratio between these two regions can be attributed to the controller as its performance measure and considered as a characteristic complementing its other linear properties.

The comparison of multidimensional stability and controllability regions can be replaced by consideration of their two-dimensional cross sections or slices. Different combinations of two-dimensional cross sections help to visualize multidimensional regions and significantly simplify the comparative analysis.

However, it should be emphasized that this comparison gives us only necessary, but not sufficient, conditions for controller assessment. The closeness of some cross sections of stability and controllability regions does not guarantee their closeness in differently oriented cross sections. Nevertheless, the proposed method provides the possibility for identification of unacceptable controllers.

The computation of two-dimensional slices of the stability region is performed by direct numerical simulation of the closed-loop system on a fine grid of points located in the two-dimensional plane. Then the slice of stability region or region of attraction is defined precisely by those points whose trajectories tend to the origin.

Similar computation of controllability region C on a grid of points is much more time consuming as it requires the solving of a two-boundary-value problem for each grid point. Fortunately, the controllability region for systems under consideration is convex, and it can be restored by computation of its boundary points in accordance with optimization approach given in Ref. 3.

The following sections of the paper present the numerical algorithm for computation of controllability region slices and provide two examples with comparative analysis of two-dimensional slices of controllability and stability region.

Computation of Controllability Region Slices

Key Idea

Two unit vectors e_i and e_j directed along ith and jth axes of coordinate system in R^{n+m} space form a basis in the slice plane $SL(i, j)$. Any point in this plane can be expressed as a linear combination of e_i and e_j:

$$SL(i, j) = \left\{ [x_0; u_0] \in R^{n+m} \quad \text{so that} \quad [x_0; u_0] = \xi_1 e_i + \xi_2 e_j \right\} \tag{5}$$

where ξ_1, ξ_2 are scalar variables.

Then the cross section $\Xi(i, j)$ of the controllability region C by plane $SL(i, j)$ in coordinates ξ_1 and ξ_2 is defined as

$$\Xi(i, j) = \left\{ \xi \in R^2 \quad \text{so that} \quad [x_0; u_0] \in SL(i, j) \cap C \right\} \tag{6}$$

where $\xi = [\xi_1, \xi_2]^T$.

From the convexity of C, it follows that $\Xi(i, j)$ is also a convex set.

The key idea of the algorithm results from the observation that each point on the boundary of the controllability region cross section is a solution of the optimization task, in which a linear function is maximized over the set of points belonging both to the controllability region and the slice plane. This idea is clearly a modification of the explicit method just described, but instead of the explicit formula in Eq. (4) the solution is based on a method of numerical optimization.

To approximate the boundary of the controllability region, let us consider a set of vectors η_l in the plane $SL(i, j)$ uniformly distributed from the center in different directions (see Fig. 1a):

$$\eta_l = [\cos\varphi_l, \sin\varphi_l]^T, \qquad \varphi_l = 2\pi l/M, \qquad l = 1, \ldots, M \tag{7}$$

Then the vectors $\xi(l)$ belonging to the boundary of the controllability region in the slice $SL(i, j)$ will be defined as the solutions of the following optimization task (see Fig. 1b):

$$\xi(l) = \arg \max_{\substack{\xi \in \Xi(i,j) \\ \xi \geq \xi_{\min} \\ \xi \leq \xi_{\max}}} \left(\eta_l^T \xi \right) \tag{8}$$

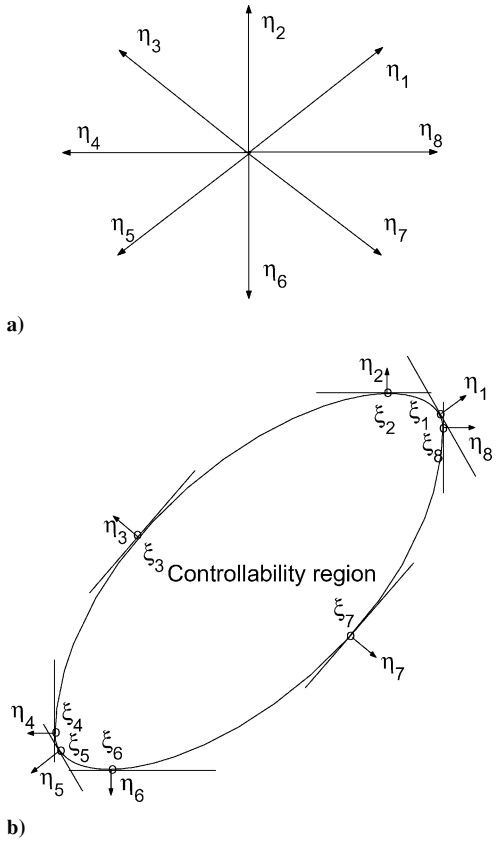

Fig. 1 Algorithm key idea: maximization of the linear function over the controllability region.

The additional constraints

$$\xi_{\min} \leq \xi \leq \xi_{\max} \tag{9}$$

are introduced in Eq. (8) to allow the computation of unbounded controllability region slices, for example, when matrix A has only one antistable eigenvalue.

The optimization task given in Eq. (8) leads us to the following variational equations:

$$\eta_l^T \xi \to \max \tag{10a}$$

$$[x_0; u_0] = \xi_1 e_i + \xi_2 e_j \tag{10b}$$

$$x_0 = -\int_0^T e^{-A\tau} B u(\tau)\, d\tau \tag{10c}$$

$$u(\tau) = u_0 + \int_0^\tau \dot{u}(t)\, dt \tag{10d}$$

$$u_{\min} \leq u(\tau) \leq u_{\max} \tag{10e}$$

$$\dot{u}_{\min} \leq \dot{u}(t) \leq \dot{u}_{\max} \tag{10f}$$

where vector ξ and function $\dot{u}(t)$ are to be determined and T is sufficiently large. The solution of the formulated optimization task in continuous time can be obtained using a version of Pontryagin's minimum principle that takes proper account of both control and state constraints. However, because of computational difficulties in application of the minimum principle we use in this paper a more simple method that is based on discrete approximation of the formulated problem.

Discretization

To solve numerically the optimization task defined by Eq. (8), the control function $u(t)$ is parameterized with sampling time ΔT,

and the system defined in Eq. (1) is treated as a discrete one. In this case the powerful linear programming methods can be applied to solve the optimization problem.

Let continuous piecewise linear control function be in the following form:

$$u(t) = u_k + \dot{u}_k(t - k\Delta T) \quad \text{for} \quad t \geq k\Delta T, \qquad t \leq (k+1)\Delta T \tag{11}$$

Here $k \geq 0$ is an integer value, $u_k \in R^m$ denotes the control vector, and $\dot{u}_k \in R^m$ denotes the vector of control inputs rates at time instant $t = k\Delta T$.

It is clear that if

$$u_{\min} \leq u_k \leq u_{\max} \tag{12a}$$

$$\dot{u}_{\min} \leq \dot{u}_k \leq \dot{u}_{\max} \tag{12b}$$

for all k, then both amplitude and rate control constraints in Eq. (2) hold for all t.

It is possible to express the state and control vectors at time instant $t = (k+1)\Delta T$ as functions of x_k, u_k, and $\dot{u}_k$ using the matrix exponential. As a result, the following discrete system is constructed:

$$x_{k+1} = Fx_k + Gu_k + H\dot{u}_k \tag{13a}$$

$$u_{k+1} = u_k + \dot{u}_k\Delta T \tag{13b}$$

where

$$F = e^{A\Delta T} \in R^{n\times n}, \qquad G = \int_0^{\Delta T} e^{A(\Delta T - \tau)}B\,\mathrm{d}\tau \in R^{n\times m}$$

$$H = \int_0^{\Delta T} e^{A(\Delta T - \tau)}B\tau\,\mathrm{d}\tau \in R^{n\times m}$$

and x_k is the system state at the time instant $t = k\Delta T$.

Prediction Equations for Discrete-Time System

The controllability or null-controllable region for the discrete system in Eq. (13) can be defined similarly to the continuous-time system case. Namely, C is the set of all extended states $[x_0; u_0]$ that can be driven to the origin by the control sequence constrained by Eq. (12).

The null-controllable region at step N, denoted as $C(N)$, is the set of extended states $[x_0; u_0]$ that can be steered to the origin with admissible control in N steps. It is clear by definition that the region $C(N)$ is a subset of the null-controllable region at time $N\Delta T$ for the continuous-time system.

As for the continuous system, all eigenvalues λ_i, $i = 1, \ldots, n$ of matrix F in Eq. (13) can be divided into stable ($|\lambda_i| < 1$), neutral ($|\lambda_i| = 1$), and antistable ($|\lambda_i| > 1$) groups. Here $|\lambda_i|$ is the complex modulus of λ_i.

The controllability region for the continuous-time system in Eq. (1) can be approximated by the null-controllable region at step N for its discrete-time counterpart in Eq. (13) with sufficiently small sampling time ΔT and large N. The number of steps N specifies the number of unknown variables in optimization procedure. For better approximation it is necessary to take N as large as possible.

The N-step solution for the discrete-time system in Eq. 13 has the following form:

$$x_N = F^N x_0 + \sum_{k=0}^{N-1} F^{N-k-1}(Gu_k + H\dot{u}_k) \tag{14a}$$

$$u_N = u_0 + \Delta T \sum_{k=0}^{N-1} \dot{u}_k \tag{14b}$$

where x_0 is the initial state vector and u_0 is the initial control vector for the discrete system.

The following combination of prediction equations (14) with control constraints (12) and terminal conditions ($x_N = 0$, $u_N = 0$) allows us to find out all initial states $[x_0; u_0] \in C(N)$ for which there exists an admissible sequence of control input rates $\dot{u}_0, \ldots, \dot{u}_{N-1}$:

$$F^N x_0 + \sum_{k=0}^{N-1} F^{N-k-1}(Gu_k + H\dot{u}_k) = 0 \tag{15a}$$

$$u_k = u_0 + \Delta T \sum_{r=0}^{k-1} \dot{u}_r, \qquad k = 1, \ldots, N \tag{15b}$$

$$u_{\min} \leq u_k \leq u_{\max}, \quad \dot{u}_{\min} \leq \dot{u}_k \leq \dot{u}_{\max}, \quad k = 0, \ldots, N-1 \tag{15c}$$

$$u_N = 0 \tag{15d}$$

Unfortunately, Eq. (15a) is ill conditioned if matrix F has antistable eigenvalues.[8] The computational difficulties in this case follow from computation of matrix F^k leading to very large errors as k increases.

When matrix F has no stable or neutral eigenvalues, Eq. (15a) can be multiplied by F^{-N} and made well conditioned:

$$x_0 = -\sum_{k=0}^{N-1} F^{-k-1}(Gu_k + H\dot{u}_k) \tag{16}$$

because matrix F^{-k} in this case has no antistable eigenvalues. However when matrix F has both stable and antistable eigenvalues, matrix F^{-k} also has both types of eigenvalues, and to improve numerical conditioning via matrix inversion is not possible any further.

In Ref. 8 a prestabilization procedure has been proposed to avoid the onset of very large errors in matrices of the form F^k. In this paper a method based on system decomposition is implemented to avoid the numerical ill-conditioning problem.

Decomposition of Discrete-Time System

There are two well-known methods suitable for system decomposition. The first one is based on the Schur decomposition, and the second one implements the block Jordan decomposition of matrix F. In this paper the Schur decomposition is used as the most robust and reliable one.[9,10]

Consider the following transformation of the state-space basis in Eq. (13):

$$x = [Q_\zeta | Q_z]\begin{bmatrix}\zeta \\ z\end{bmatrix} \tag{17}$$

so that $[Q_\zeta | Q_z]^T [Q_\zeta | Q_z] = I$. The columns of $Q_\zeta \in R^{n\times(n-q)}$ span the subspace V_ζ associated with $(n-q)$ stable and neutral eigenvalues, while the columns of $Q_z \in R^{n\times q}$ span the subspace V_z, which is a complementary subspace of V_ζ. Note that $V_z \cup V_\zeta = R^n$ and V_ζ is an F-invariant subspace, that is, from $x \in V_\zeta$ it follows that $Fx \in V_\zeta$.

In the new basis the open-loop system in Eq. (13) is represented as

$$\begin{bmatrix}\zeta_{k+1} \\ z_{k+1}\end{bmatrix} = Q^T F Q \begin{bmatrix}\zeta_k \\ z_k\end{bmatrix} + Q^T G u_k + Q^T H \dot{u}_k$$

$$= \begin{bmatrix} Q_\zeta^T F Q_\zeta & Q_\zeta^T F Q_z \\ 0_{q\times(n-q)} & Q_z^T F Q_z \end{bmatrix}\begin{bmatrix}\zeta_k \\ z_k\end{bmatrix}$$

$$+ \begin{bmatrix} Q_\zeta^T G \\ Q_z^T G \end{bmatrix} u_k + \begin{bmatrix} Q_\zeta^T H \\ Q_z^T H \end{bmatrix}\dot{u}_k \tag{18}$$

where matrix $Q_\zeta^T F Q_\zeta$ has only stable and neutral eigenvalues, matrix $Q_z^T F Q_z$ has only antistable eigenvalues, and together these eigenvalues form the whole spectrum of eigenvalues for matrix F.

Note that z_k dynamics associated with q antistable eigenvalues is decoupled from ζ_k and described by the following open-loop subsystem:

$$z_{k+1} = F_z z_k + G_z u_k + H_z \dot{u}_k \tag{19}$$

where $F_z = Q_z^T F Q_z \in R^{q\times q}$, $G_z = Q_z^T G \in R^{q\times m}$, $H_z = Q_z^T H \in R^{q\times m}$, and $z_k = Q_z^T x_k$.

In a similar way the transformation of the state-space basis can decouple the dynamics associated with stable and neutral eigenvalues. Consider the following transformation of the basis in Eq. (13):

$$x = [Q_w | Q_s] \begin{bmatrix} w \\ s \end{bmatrix} \tag{20}$$

so that $[Q_w|Q_s]^T[Q_w|Q_s] = I$. The columns of $Q_w \in R^{n\times q}$ span the subspace V_w associated with q antistable eigenvalues, and the columns of $Q_s \in R^{n\times(n-q)}$ span the complementary subspace V_s of V_w. Obviously, $V_w \cup V_s = R^n$ and V_w is an F-invariant subspace.

Dynamics associated with the stable and neutral eigenvalues s_k can be isolated similarly to antistable eigenvalues case [see Eq. (19)]:

$$s_{k+1} = F_s s_k + G_s u_k + H_s \dot{u}_k \tag{21}$$

where $F_s = Q_s^T F Q_s \in R^{(n-q)\times(n-q)}$, $G_s = Q_s^T G \in R^{(n-q)\times m}$, $H_s = Q_s^T H \in R^{(n-q)\times m}$, and $s_k = Q_s^T x_k$.

Numerically Robust Solution via Linear Programming

The decomposed subsystems for antistable and stable/neutral subspaces [see Eqs. (19) and (21)] allow the construction of well-conditioned prediction equations for z and s, respectively:

$$F_z^{-N} z_N = z_0 + \sum_{k=0}^{N-1} F_z^{-k-1}(G_z u_k + H_z \dot{u}_k) \tag{22a}$$

$$s_N = F_s^N s_0 + \sum_{k=0}^{N-1} F_s^{N-k-1}(G_s u_k + H_s \dot{u}_k) \tag{22b}$$

The underlying idea here is that matrices F_z^{-k} and F_s^k are well-conditioned because both F_z^{-1} and F_s do not contain antistable eigenvalues and large errors in F_z^{-k} and F_s^k do not appear.

Note that the evolution of the full state vector x_k is completely defined by the evolution of the subsystems states s_k and z_k.

The ultimate goal of the computational algorithm is to maximize the following scalar function for every given vector $\eta_l \in R^2$ in the slice plane $SL(i, j)$:

$$\eta_l^T \xi \to \max \tag{23}$$

so that points $[x_0; u_0] = \xi_1 e_i + \xi_2 e_j$ belong to the controllability region $C(N)$. The resulting vector $\xi(l)$ will define a point on the boundary of the controllability region [see Eq. (8)].

To specify this optimization problem, we need to combine the well-conditioned prediction equations (22) with terminal conditions $s_N = 0$ and $z_N = 0$, add initial conditions $s_0 = Q_s^T x_0$ and $z_0 = Q_z^T x_0$ and control constraints (12), and confine the allowable area in the plane $SL(i, j)$ to consider unbounded controllability regions. All of these form the following set of linear constraints:

$$Q_z^T(\xi_1 e_{xi} + \xi_2 e_{xj}) = -\sum_{k=0}^{N-1} F_z^{-k-1}(G_z u_k + H_z \dot{u}_k) \tag{24a}$$

$$F_s^N Q_s^T(\xi_1 e_{xi} + \xi_2 e_{xj}) = -\sum_{k=0}^{N-1} F_s^{N-k-1}(G_s u_k + H_s \dot{u}_k) \tag{24b}$$

$$u_k = u_0 + \Delta T \sum_{r=0}^{k-1} \dot{u}_r, \qquad k = 1, \ldots, N \tag{24c}$$

$$u_0 = \xi_1 e_{ui} + \xi_2 e_{uj}, \qquad u_N = 0 \tag{24d}$$

$$u_{\min} \le u_k \le u_{\max}, \qquad \dot{u}_{\min} \le \dot{u}_k \le \dot{u}_{\max} \qquad k = 0, \ldots, N-1 \tag{24e}$$

$$\xi_{\min} \le \xi \le \xi_{\max} \tag{24f}$$

where unit vector $e_i \in R^{n+m}$ is resolved on the state ($e_{xi} \in R^n$) and the control ($e_{ui} \in R^m$) vector components: $e_i = [e_{xi}; e_{ui}]$.

The unknown variables in the set of linear constraints in Eqs. (24) are the coordinate vector in the slice plane $\xi = [\xi_1, \xi_2]^T$ and the control rate vectors $\dot{u}_k$, $k = 0, \ldots, N-1$.

The optimization problem just formulated can be effectively solved by a linear programming method.

Computational Issues

The proposed algorithm has been implemented as a MATLAB® function, which can be freely requested from the authors. All computational results presented in this paper have been obtained using MATLAB 6.5 on a personal computer Pentium IV 1.6 GHz. For example, the computation of the boundary of the controllability region for an eight-dimensional dynamical system considered as an example in the next section takes 20 s when $N = 100$. (Only amplitude constraints have been imposed.) For the Schur decomposition of the discrete systems, the function *blkrsch* from the Robust Control Toolbox has been used. The linear programming has been performed by the function *linprog* (large-scale algorithm) from the Optimization Toolbox.

Numerical Examples

Example 1: Controllability Regions Beyond the Flutter Boundary

The active flutter suppression problem has been intensively investigated with implementation of different control design techniques.[11–19] Different linear and nonlinear controllers applied for flutter suppression improve the system dynamic responses and extend the flutter boundary. However, these approaches have difficulty when realistic constraints are imposed on the maximum rate and deflection of the control surfaces used for flutter control.[11] It is indicated[11] that there exists some limit in terms of dynamic pressure or flow speed for possible delay of the flutter onset in the closed-loop system.

This fact can be related to the size of the controllability region for the open-loop system beyond the flutter boundary. Because of limited authority of control effectors, the size of the controllability region decreases with increase of system instability and can become critical against the available level of external disturbances.

A more deep insight into the active flutter suppression problem will require a detailed analysis of the controllability regions for the open-loop system and regions of attraction for the closed-loop system. Such analysis will help to improve the control laws design and provide the realistic level of robustness for active control flutter suppression system.

To elucidate the proposed approach, we consider hereafter an airfoil with trailing-edge flap, which can be treated as a typical wing section (see Fig. 2).

The dynamic equations of this aeroservoelastic system can be represented in the following matrix form[12,18,20]:

$$\begin{bmatrix} m_a & s_{h\theta} & s_{h\delta} \\ s_{h\delta} & I_\theta & s_{\theta\delta} \\ s_{h\delta} & s_{\theta\delta} & I_\delta \end{bmatrix} \begin{bmatrix} \ddot{h} \\ \ddot{\theta} \\ \ddot{\delta} \end{bmatrix} + \begin{bmatrix} k_h & 0 & 0 \\ 0 & k_\theta & 0 \\ 0 & 0 & k_\delta \end{bmatrix} \begin{bmatrix} h \\ \theta \\ \delta \end{bmatrix}$$

$$= \begin{bmatrix} 0 \\ 0 \\ k_\delta \end{bmatrix} \delta_c + \begin{bmatrix} c_h(\rho U^2/2)S \\ c_m(\rho U^2/2)S\bar{c} \\ c_\delta(\rho U^2/2)S\bar{c} \end{bmatrix} \tag{25}$$

where the nondimensional aerodynamic coefficients for the normal force c_h, the pitch moment c_m, and the flap hinge moment c_δ are expressed as linear functions of $\ddot{\theta}$, $\dot{\theta}$, θ, $\ddot{h}$, $\dot{h}$, h, $\ddot{\delta}$, $\dot{\delta}$, δ, and unsteady aerodynamic contribution to the normal force coefficient c_w, generated by trailing-edge vortex wake.[20]

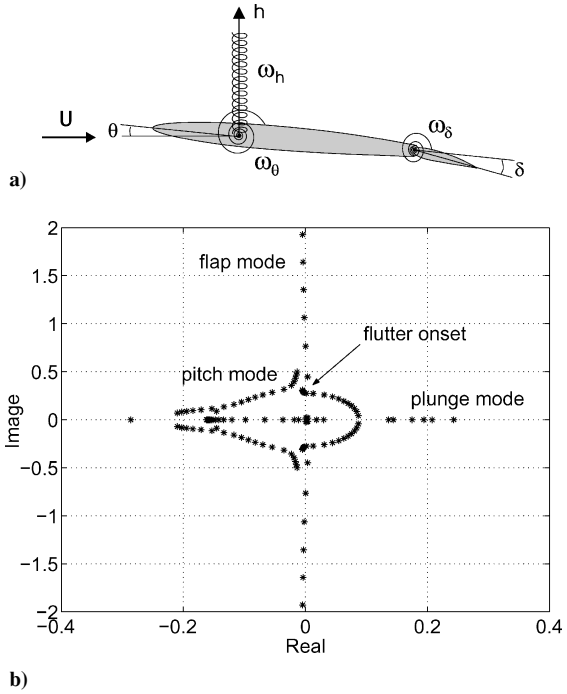

Fig. 2 Sketch of a) the aeroservoelastic airfoil system and b) the root loci for different reduced frequencies in pitch.

The unsteady aerodynamic term c_w is replaced with a sum of two dynamic variables x_7 and x_8, governed by the first-order differential equations with characteristic timescales identified from approximation of the Theodorsen transfer function.[18,20]

The system (25) in its nondimensional form is supplemented with two first-order unsteady aerodynamic equations. And the final eight-dimensional dynamic system is represented in the state-space form given in Eq. (1) with the state vector $x = [\bar{h}, \bar{h}, \theta, \dot{\theta}, \delta, \dot{\delta}, x_7, x_8]^T$, where $\bar{h} = h/\bar{c}$. The reduced natural frequencies of the system in the pitch, plunge, and flap modes are described here: $\omega_\theta = \sqrt{(k_\theta/l_\theta)}\bar{c}/(2U)$, $\omega_{\theta_{\text{fl}}} = 0.33$, $\omega_h = 0.8\omega_\theta$, and $\omega_\delta = 10\omega_\theta$.

Matrices A and B and the open-loop system eigenvalues for the aeroservoelastic system are presented in Appendix for several values of the natural frequency in pitch ω_θ, which is inversely proportional to flow speed as just described. The flap mode natural frequency ω_δ in the considered case is much higher than the natural frequency ω_θ, and the plunge mode natural frequency ω_h is approximately of the same order.

The root locus of the aeroservoelastic open-loop system for various values of reduced frequency ω_θ is shown in Fig. 2 (bottom plot). The plunge mode eigenvalues become unstable at $\omega_\theta \le \omega_{\theta\text{fl}}$, and their real parts increase with decrease of ω_θ (or increase of flow speed U). At the same time the pitch mode eigenvalues become more stable.

The numerical algorithm outlined in the preceding section has been applied for computation of controllability regions of aeroservoelastic airfoil system within the flutter range at $\omega_\theta \le \omega_{\theta\text{fl}}$.

Figure 3 shows the computed two-dimensional slices of the multidimensional controllability regions in the planes $(\bar{h}, \dot{\bar{h}})$ and $(\dot{\theta}, \theta)$. (Note that all other state variables are equal to zero.) Only deflection constraint $|\delta_c| \le 0.1$ rad has been imposed in this example.

At the flutter boundary $\omega_\theta = \omega_{\theta\text{fl}}$ the system is still controllable in the whole state space. However, as soon as the operational parameter crosses the linear flutter boundary and the level of linear system instability increases the controllability region decreases significantly.

First, the controllability regions have the elliptical cross sections in both planes. When the imaginary part of antistable eigenvalues drops ≈0.08, the controllability regions are stretched into a narrow strip. The length of these strip regions increases when two eigenvalues of antistable subsystem become real.

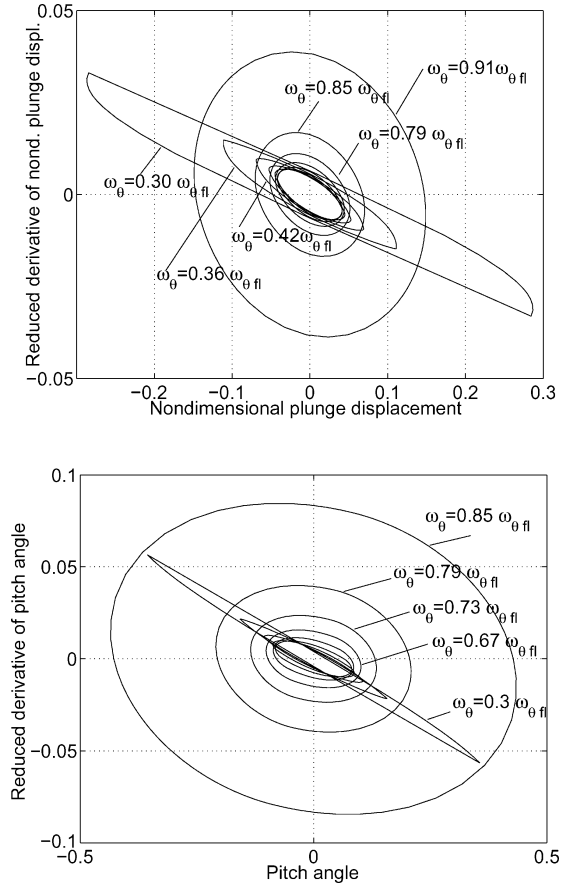

Fig. 3 Slices of the controllability regions computed for the flutter range of ω_θ under deflection limit $|\delta_c| \le 0.1$ rad.

The size of the controllability region slice, for example, at $\omega_\theta = 0.67\omega_{\theta\text{fl}}$ allows the maximum disturbances in pitch angle $|\theta| \le 0.1$ rad and in nondimensional plunge displacement $|\bar{h}| \le 0.03$. It means that if external disturbances, such as the atmospheric turbulence or wind gust, lead to higher level of perturbations there is no possibility to keep the system stable using any controller.

Note that the rate constraint produces additional reduction in the controllability region size. In Fig. 4a the cross sections of the controllability region are presented for different deflection rate limits.

The area of the controllability region cross sections clearly tends to zero as the rate limit decreases significantly. At $|\dot{\delta}_c| \ge 0.05$ rad the cross-section area approaches the size defined only by deflection limit constraints. So the computation of the controllability region as a function of the deflection and rate limits can be useful for specification of important requirements for actuator characteristics (see Fig. 4b).

The stability region of the closed-loop system is normally less than the open-loop system controllability region. Only the stability-optimal controller can enlarge the stability region up to the controllability region size.[4,5]

As an example, Fig. 5 presents comparisons of the open-loop controllability region and the closed-loop stability region slices for the linear system at operational point $\omega_\theta = 0.67\omega_{\theta\text{fl}}$ with two different controllers. In both cases the applied feedback is in the form of linear state control law, supplemented with simple saturation function:

$$\delta_c(t) = \text{sat}(Kx) \tag{26}$$

where $K \in R^{1\times n}$,

$$\text{sat}(u) = \begin{cases} u_{\max}, & \text{if} \quad u > u_{\max} \\ u, & \text{if} \quad u_{\min} \le u \le u_{\max} \\ u_{\min}, & \text{if} \quad u < u_{\min} \end{cases} \tag{27}$$

and $u_{\max} = -u_{\min} = 0.1$ rad.

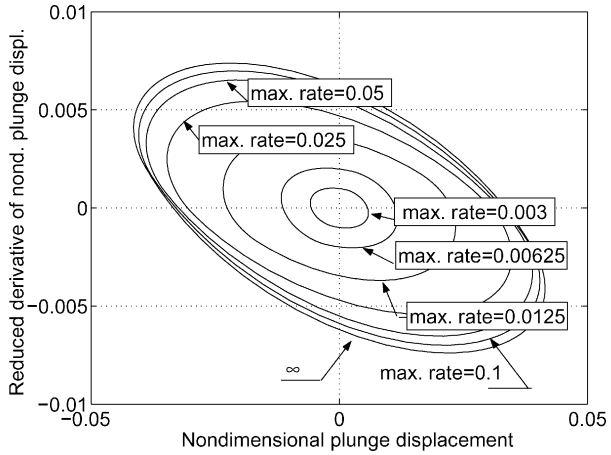

Fig. 4a Controllability region slices at $\omega_\theta = 0.67\omega_{\theta\text{fl}}$ for different rate limits.

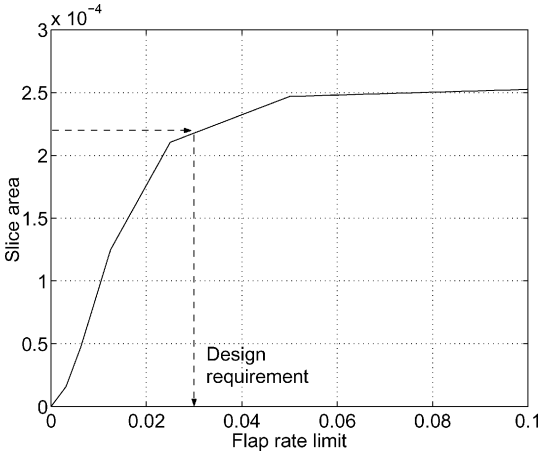

Fig. 4b Area of these slices vs the rate limit. The deflection limit $|\delta_c| \le 0.1$ rad.

In the first case, the feedback gain K is selected for the pole placement controller, which transforms the unstable complex pair $0.0632 \pm 0.1994i$ to the stable one $-0.12 \pm 0.4i$ (see Fig. 5a). As one can see, the size of the closed-loop system stability region slice in this case is approximately two times smaller than the size of the open-loop controllability region slice.

In the second case the system is closed by the linear-quadratic (LQ) controller, where the feedback coefficient vector K was obtained as the solution for the problem of minimization of the performance index

$$J = \int_0^\infty (x^T x + u^T u)\,\mathrm{d}t$$

In this case the closed-loop system stability region slice is very close to the open-loop controllability region slice.

Example 2: Controllability Regions for the X-33 Vehicle

Another example of the constrained stabilization problem is connected with unstable lateral/directional dynamics of the X-33 vehicle[21] at critical conditions during the entry flight: altitude 29,624 m, Mach number 3.13 with trim angle of attack $\alpha = 0.109$ rad, and zero trim sideslip and bank angles.

The eight control surfaces can operate independently, and their perturbations from the trim values form the control vector for the linearized system in Eq. (1):

$$u = [\delta_{\text{revi}}, \delta_{\text{levi}}, \delta_{\text{rbf}}, \delta_{\text{lbf}}, \delta_{\text{rvr}}, \delta_{\text{lvr}}, \delta_{\text{revo}}, \delta_{\text{levo}}]^T$$

The control surface limits are given in Table 1.

Table 1 X-33 control surface limits

Control surface	Lower bound, rad	Upper bound, rad
δ_{revi}	−0.4363	0.4363
δ_{levi}	−0.4363	0.4363
δ_{rbf}	−0.3054	0.4101
δ_{lbf}	−0.3054	0.4101
δ_{rvr}	−0.5236	0.5236
δ_{lvr}	−0.5236	0.5236
δ_{revo}	−0.4363	0.4363
δ_{levo}	−0.4363	0.4363

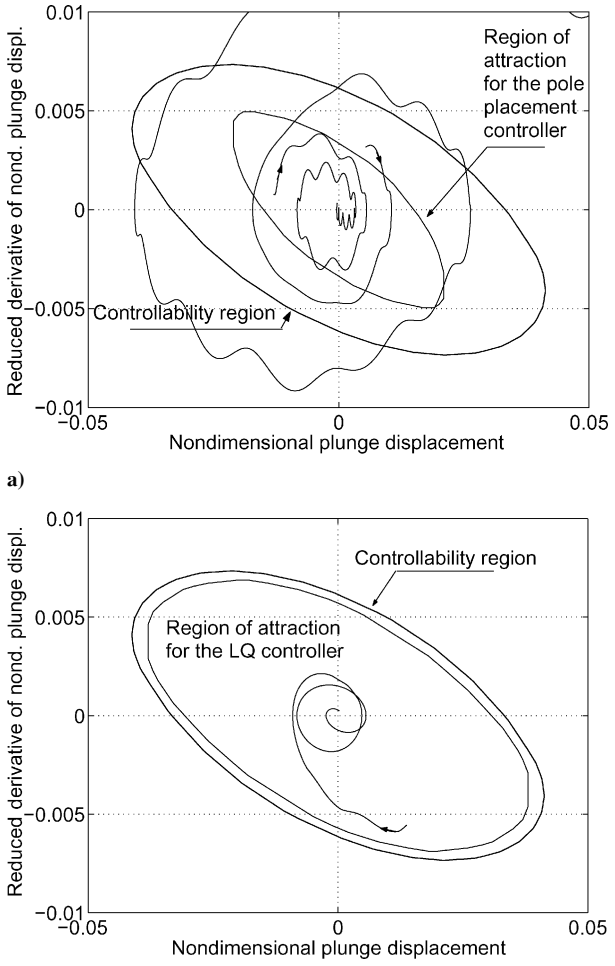

Fig. 5 Comparison of the controllability region at $\omega_\theta = 0.67\omega_{\theta\text{fl}}$ with the regions of attraction for the closed-loop system: a) slices for the pole placement controller and b) for the linear-quadratic controller. The deflection limit $|\delta_c| \le 0.1$ rad.

The state vector in the system defined by Eq. (1) combines the longitudinal and lateral/directional motion parameters:

$$x = [P, R, \beta, \phi, \psi, \alpha, Q, \theta, V]^T$$

The matrices of the linearized X-33 vehicle at the preceding flight conditions are given in Ref. 21. Table 2 shows the open-loop poles. Note that the first five eigenvalues represent the lateral/directional dynamics and the last four eigenvalues represent the longitudinal dynamics.

Although the linearized longitudinal and lateral/directional motions are decoupled in the matrix A, all control surfaces in different extent contribute both to longitudinal and lateral/directional dynamics. Hence the control law design must be carried out simultaneously for longitudinal and lateral modes.[21]

There are two unstable eigenvalues in the system; the most significant λ_2 is produced because of directional aerodynamic instability,

Table 2 Eigenvalues of the X-33 model

Open loop	Closed loop
$\lambda_1 = -1.0007$	$-0.4 + 1.25i$
$\lambda_2 = 0.93495$	$-0.4 - 1.25i$
$\lambda_3 = -0.102$	-0.102
$\lambda_4 = -0.000562$	-0.0562
$\lambda_5 = 0$	-0.01
$\lambda_6 = -0.0609 + 1.24i$	$-0.0609 + 1.24i$
$\lambda_7 = -0.0609 - 1.24i$	$-0.0609 - 1.24i$
$\lambda_8 = -0.0149$	-0.0149
$\lambda_9 = 0.000646$	-0.0646

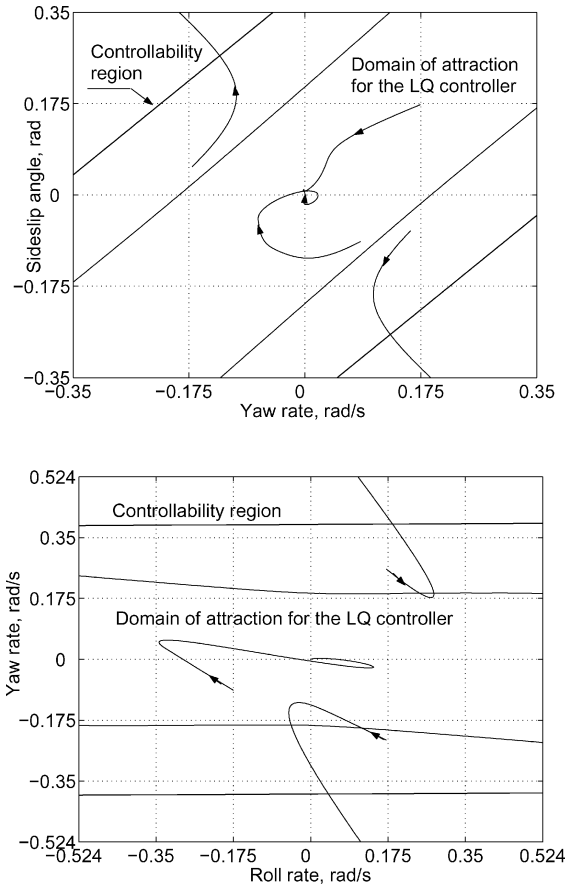

Fig. 6 X-33 linearized model. Comparison of controllability and stability region cross sections at the presence of only deflection constraints: the LQ controller.

and the second one λ_9 is a very slow phugoid mode instability in the longitudinal motion. The controllability region slices in the planes (β, P) and (R, P) of the lateral/directional parameters have the form of a strip (see Figs. 6–8).

The controllability region cross sections have been first computed without account of the rate constraints. And the two stabilizing control laws, the LQ optimal controller (designed in the same manner as for the aeroservoelastic problem in the preceding section) and the pole placement controller, have been compared in terms of slices of their closed-loop stability regions.

To take into account control constraints, the saturation function given in Eq. (27) was implemented for each control input. The slice of the domain of attraction for the LQ optimal controller covers a large part of the controllability region slice, as shown in Fig. 6. In Fig. 7 the cross sections of the closed-loop system stability region are shown for the pole placement controller. The closed-loop system eigenvalues in this case have been assigned as shown in Table 2. Note that during control synthesis only body flaps have been considered as active.

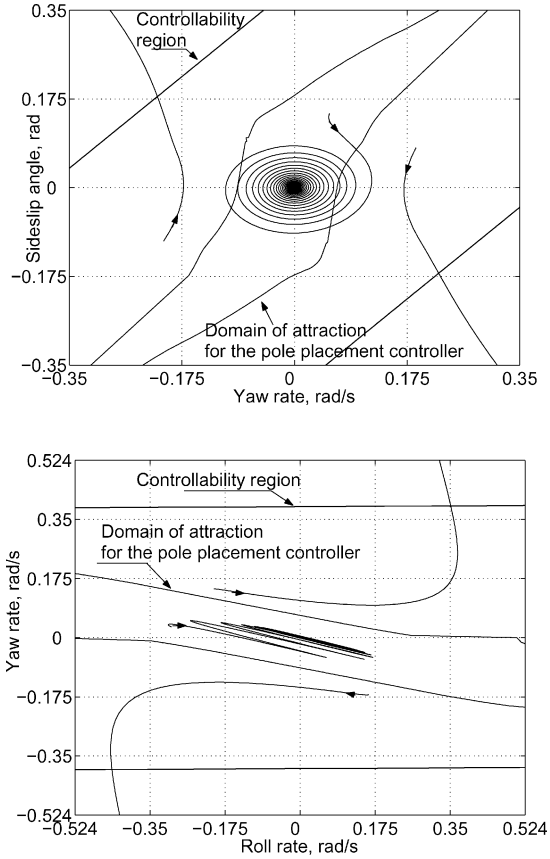

Fig. 7 X-33 linearized model. Comparison of controllability and stability region cross sections at the presence of only deflection constraints: the pole placement controller.

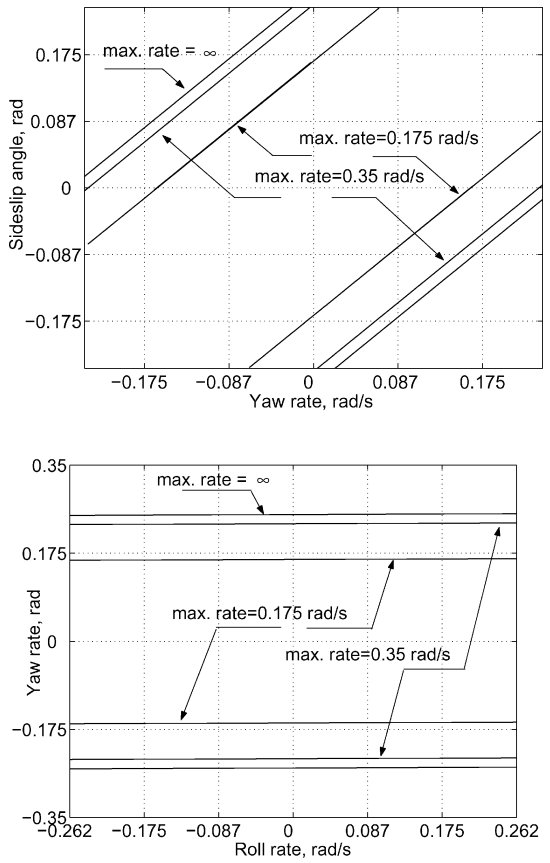

Fig. 8 X-33 linearized model. Comparison of controllability region cross sections for different rate limits.

Presented results demonstrate that in the both cases the closed-loop system stability regions are less than the controllability region. The pole placement control law can produce unsatisfactory size of the stability region for the closed-loop system when the assigned locations of the closed-loop eigenvalues are taken without consideration of the stability region size.

To demonstrate the rate limit influence on the controllability region size, the absolute values of rates for all control effectors have been limited by the same value. The cross sections of the controllability region in the planes (β, P) and (R, P) for maximum rate limit 0.35 and 0.175 rad/s are shown in Fig. 8. One can see that even these very slow actuators are not very critical in terms of the size of the controllability region because the decrease of the controllability region slice caused by rate saturation in this case is relatively small.

Conclusions

The proposed numerical algorithm for computation of the controllability regions for unstable linear systems with two types of control constraints such as deflection limit and rate saturation can be applied for postdesign assessment of different control laws and specification of design requirements for actuator characteristics. This method allows the unlimited number of control effectors and antistable eigenvalues in the open-loop system. The presented computational examples for simple aeroservoelastic system and the aerodynamically unstable X-33 vehicle demonstrate the utility of the proposed method for design and postdesign assessment of control laws at flight regimes with unstable dynamics.

Appendix: Linearized Equations of the Aeroservoelastic Airfoil System

Matrices A with their eigenvalues λ and matrices B of the linearized aeroservoelastic airfoil system (1) are presented next for four different operational conditions beyond the flutter boundary $\omega_\theta = \omega_{\theta_{\text{fl}}}$.

1) $\omega_\theta = 0.9\omega_{\theta_{\text{fl}}}$

$$A = \begin{bmatrix} 0 & 1.0000 & 0 & 0 & 0 & 0 & 0 & 0 \\ -0.0849 & -0.0167 & -0.0105 & 0.0095 & 0.0186 & 0.0009 & 0.0053 & 0.0053 \\ 0 & 0 & 0 & 1.0000 & 0 & 0 & 0 & 0 \\ -0.1416 & -0.0387 & -0.1820 & -0.0147 & 1.8038 & -0.0034 & 0.0123 & 0.0123 \\ 0 & 0 & 0 & 0 & 0 & 1.0000 & 0 & 0 \\ 0.0351 & 0.0706 & 0.7735 & 0.1260 & -17.4331 & 0.0009 & -0.0225 & -0.0225 \\ 0 & -1.1944 & 1.1944 & 0.5375 & 0.6567 & 0.0888 & -0.8598 & 0 \\ 0 & -0.2932 & 0.2932 & 0.1319 & 0.1612 & 0.0218 & 0 & -0.1673 \end{bmatrix} \quad B = \begin{bmatrix} 0 \\ -0.0146 \\ 0 \\ -1.8250 \\ 0 \\ 17.5566 \\ 0 \\ 0 \end{bmatrix} \quad \lambda = \begin{bmatrix} -0.0057 \pm 4.1852i \\ -0.0351 \pm 0.3166i \\ 0.0128 \pm 0.2722i \\ -0.1563 \\ -0.8453 \end{bmatrix}$$

2) $\omega_\theta = 0.67\omega_{\theta_{\text{fl}}}$

$$A = \begin{bmatrix} 0 & 1.0000 & 0 & 0 & 0 & 0 & 0 & 0 \\ -0.0457 & -0.0167 & 0.0021 & 0.0095 & 0.0118 & 0.0009 & 0.0053 & 0.0053 \\ 0 & 0 & 0 & 1.0000 & 0 & 0 & 0 & 0 \\ -0.0762 & -0.0387 & -0.0800 & -0.0147 & 0.9603 & -0.0034 & 0.0123 & 0.0123 \\ 0 & 0 & 0 & 0 & 0 & 1.0000 & 0 & 0 \\ 0.0189 & 0.0706 & 0.3834 & 0.1260 & -9.3181 & 0.0009 & -0.0225 & -0.0225 \\ 0 & -1.1944 & 1.1944 & 0.5375 & 0.6567 & 0.0888 & -0.8598 & 0 \\ 0 & -0.2932 & 0.2932 & 0.1319 & 0.1612 & 0.0218 & 0 & -0.1673 \end{bmatrix} \quad B = \begin{bmatrix} 0 \\ -0.0079 \\ 0 \\ -0.9814 \\ 0 \\ 9.4415 \\ 0 \\ 0 \end{bmatrix} \quad \lambda = \begin{bmatrix} -0.0053 \pm 3.0595i \\ 0.0632 \pm 0.1944i \\ -0.0935 \pm 0.2096i \\ -0.1420 \\ -0.8442 \end{bmatrix}$$

3) $\omega_\theta = 0.42\omega_{\theta_{\text{fl}}}$

$$A = \begin{bmatrix} 0 & 1.0000 & 0 & 0 & 0 & 0 & 0 & 0 \\ -0.0185 & -0.0167 & 0.0108 & 0.0095 & 0.0071 & 0.0009 & 0.0053 & 0.0053 \\ 0 & 0 & 0 & 1.0000 & 0 & 0 & 0 & 0 \\ -0.0308 & -0.0387 & -0.0094 & -0.0147 & 0.3763 & -0.0034 & 0.0123 & 0.0123 \\ 0 & 0 & 0 & 0 & 0 & 1.0000 & 0 & 0 \\ 0.0077 & 0.0706 & 0.1133 & 0.1260 & -3.7000 & 0.0009 & -0.0225 & -0.0225 \\ 0 & -1.1944 & 1.1944 & 0.5375 & 0.6567 & 0.0888 & -0.8598 & 0 \\ 0 & -0.2932 & 0.2932 & 0.1319 & 0.1612 & 0.0218 & 0 & -0.1673 \end{bmatrix} \quad B = \begin{bmatrix} 0 \\ -0.0032 \\ 0 \\ -0.3974 \\ 0 \\ 3.8234 \\ 0 \\ 0 \end{bmatrix} \quad \lambda = \begin{bmatrix} -0.0043 \pm 1.9276i \\ 0.0842 \pm 0.0865i \\ -0.1531 \pm 0.1154i \\ -0.0665 \\ -0.8445 \end{bmatrix}$$

4) $\omega_\theta = 0.3\omega_{\theta_{\text{fl}}}$

$$A = \begin{bmatrix} 0 & 1.0000 & 0 & 0 & 0 & 0 & 0 & 0 \\ -0.0094 & -0.0167 & 0.0137 & 0.0095 & 0.0056 & 0.0009 & 0.0053 & 0.0053 \\ 0 & 0 & 0 & 1.0000 & 0 & 0 & 0 & 0 \\ -0.0157 & -0.0387 & 0.0142 & -0.0147 & 0.1816 & -0.0034 & 0.0123 & 0.0123 \\ 0 & 0 & 0 & 0 & 0 & 1.0000 & 0 & 0 \\ 0.0039 & 0.0706 & 0.0232 & 0.1260 & -1.8273 & 0.0009 & -0.0225 & -0.0225 \\ 0 & -1.1944 & 1.1944 & 0.5375 & 0.6567 & 0.0888 & -0.8598 & 0 \\ 0 & -0.2932 & 0.2932 & 0.1319 & 0.1612 & 0.0218 & 0 & -0.1673 \end{bmatrix} \quad B = \begin{bmatrix} 0 \\ -0.0016 \\ 0 \\ -0.2028 \\ 0 \\ 1.9507 \\ 0 \\ 0 \end{bmatrix} \quad \lambda = \begin{bmatrix} -0.0029 \pm 1.3548i \\ -0.1844 \pm 0.0952i \\ 0.1443 \\ 0.0302 \\ -0.0110 \\ -0.8463 \end{bmatrix}$$

Acknowledgments

This research was funded in part by QinetiQ, Ltd., United Kingdom, and monitored by Yoge Patel and Ian Kaynes. This support is gratefully appreciated. The authors also thank the reviewers for their valuable comments.

References

[1]Hanson, G. D., and Stengel, R. F., "Effects of Displacement and Rate Saturation on the Control of Statically Unstable Aircraft," *Journal of Guidance, Control, and Dynamics*, Vol. 7, No. 2, 1984, pp. 197–205.

[2]Shrivastava, P. C., and Stengel, R. F., "Stability Boundaries for Aircraft with Unstable Lateral-Directional Dynamics and Control Saturation," *Journal of Guidance, Control, and Dynamics*, Vol. 12, No. 1, 1989, pp. 62–70.

[3]Formal'skii, A. M., "Controllability Domain of Systems Having Limited Control Resources," *Automation and Remote Control*, Vol. 29, No. 3, 1968, pp. 375–382.

[4]Goman, M., Fedulova, E., and Khramtsovsky, A., "Maximum Stability Region Design for Unstable Aircraft with Control Constraints," AIAA Paper 96-3910, July 1996.

[5]Hu, T., and Lin, Z., *Control Systems with Actuator Saturation: Analysis and Design*, Birkhäuser, Boston, 2001, Chap. 2.

[6]Goman, M. G., and Demenkov, M. N., "Stabilization of Unstable Aircraft Dynamics Under Control Constraints," *Advances in Dynamics and Control*, edited by S. Sivasundaram, CRC Press, Boca Raton, FL, 2004, Chap. 8.

[7]Pontryagin, L. S., Boltyanskii, V. G., Gamkrelidze, R. V., and Mishchenko, E. F., *The Mathematical Theory of Optimal Processes*, Wiley, New York, 1962, pp. 127–130.

[8]Rossiter, J. A., Kouvaritakis, B., and Rice, M. J., "A Numerically Robust State-Space Approach to Stable-Predictive Control Strategies," *Automatica*, Vol. 34, No. 1, 1998, pp. 65–73.

[9]Golub, G. H., and Van Loan, C. F., *Matrix Computations*, North Oxford Academic, London, 1986, pp. 240–242.

[10]Castelan, E. B., Gomes da Silva, J. M., Jr., and Cury, J. E. R., "A Reduced-Order Framework Applied to Linear Systems with Constrained Controls," *IEEE Transactions on Automatic Control*, Vol. 41, No. 2, 1996, pp. 249–255.

[11]Friedmann, P. P., "Renaissance of Aeroelasticity and Its Future," *Journal of Aircraft*, Vol. 36, No. 1, 1999, pp. 105–121.

[12]Waszak, M. R., "Modeling the Benchmark Active Control Technology Wind-Tunnel Model for Active Control Design Applications," NASA TP-1998-206270, June 1998.

[13]Waszak, M. R., "Robust Multivariable Flutter Suppression for the Benchmark Active Control Technology Wind Tunnel Model," *Journal of Guidance, Control, and Dynamics*, Vol. 24, No. 1, 2001, pp. 147–153.

[14]Mukhopadhyay, V., "Transonic Flutter Suppression Control Law Design and Wind-Tunnel Test Results," *Journal of Guidance, Control, and Dynamics*, Vol. 23, No. 5, 2000, pp. 930–937.

[15]Frampton, K. D., and Clark, R. L., "Experiments on Control of Limit-Cycle Oscillations in a Typical Section," *Journal of Guidance, Control, and Dynamics*, Vol. 23, No. 5, 2000, pp. 956–960.

[16]Scott, R. C., and Pado, L. E., "Active Control of Wind Tunnel Model Aeroelastic Response Using Neural Networks," *Journal of Guidance, Control, and Dynamics*, Vol. 23, No. 6, 2000, pp. 1100–1108.

[17]Ko, J., Strganac, T. W., and Kurdila, A. J., "Stability and Control of a Structurally Nonlinear Aeroelastic System," *Journal of Guidance, Control, and Dynamics*, Vol. 21, No. 5, 1998, pp. 718–725.

[18]Block, J. J., and Strganac, T. W., "Applied Active Control for a Nonlinear Aeroelastic Structure," *Journal of Guidance, Control, and Dynamics*, Vol. 21, No. 6, 1998, pp. 838–845.

[19]Mukhopadhyay, V., "Historical Perspective on Analysis and Control of Aeroelastic Responses," *Journal of Guidance, Control, and Dynamics*, Vol. 26, No. 5, 2003, pp. 673–684.

[20]Goman, M., Khrabrov, A., and Khramtsovsky, A., "Stability and Bifurcation Analysis of an Aeroelastic Airfoil System," DERA, Contract Rept. CU004-07770, Farnborough, UK, Sept. 2001.

[21]Burken, J. J., Lu, P., and Wu, Z., "Reconfigurable Flight Control Designs with Application to the X-33 Vehicle," NASA TM-1999-206582, Aug. 1999.